JOURNAL OF GEOPHYSICAL RESEARCH, VOL. 102, NO. A4, PAGES 7267-7277, APRIL 1, 1997

Comparison of models and measurements at Millstone Hill during the January 24–26, 1993, minor storm interval

M. J. Buonsanto,[1] M. Codrescu,[2] B. A. Emery,[3] C. G. Fesen,[4,5] T. J. Fuller-Rowell,[2] D. J. Melendez-Alvira,[6] and D. P. Sipler[1]

Abstract. Results from four first-principle models are compared with Millstone Hill incoherent scatter radar and Fabry-Perot interferometer measurements taken during January 24–26, 1993, a period which included a minor geomagnetic storm. The models used in this study are the thermosphere ionosphere electrodynamics general circulation model (TIEGCM) with and without forcings from the assimilative mapping of ionospheric electrodynamics (AMIE) technique, the coupled thermosphere ionosphere model (CTIM), and the field line interhemispheric plasma (FLIP) model. The present study is the first time the AMIE inputs have been used in the TIEGCM model. TIEGCM and CTIM both underestimate the neutral temperature because of an underestimation of the Joule heating rate. An increase in the high latitude Joule heating would modify the thermospheric circulation. This could result in increases in N_2 and O_2 density above Millstone Hill, which would decrease the AMIE TIEGCM peak electron density (NmF_2) to agree better with the observations, but would result in poorer agreement between CTIM and the data. The FLIP model NmF_2 is a little low compared to the data, perhaps because of an inadequacy of the mass spectrometer incoherent scatter (MSIS) 86 model composition or the H^+ flux in the model. Good agreement is obtained between atomic oxygen density [O] given by MSIS and [O] obtained from the radar data using a heat balance equation, provided an O^+–O collision frequency factor of 1.3 is used. While the TIEGCM underestimates the electron and ion temperatures, the FLIP model reproduces major features of the data, apart from a large nighttime enhancement in T_e. During the minor storm interval the observed neutral winds show alternating equatorward surges and abatements apparently due to passage of traveling atmospheric disturbances (TADs) seen in the model results. These are associated with a late evening increase observed in NmF_2 accompanied by a large increase in F_2 peak height (hmF_2). These perturbations in NmF_2 and hmF_2 are not reproduced by the TIEGCM or CTIM. The NmF_2 increase may be due to a decrease in O^+ recombination rate caused by the higher hmF_2, combined with compressional effects of a TAD and an enhanced downward flux of O^+ ions.

1. Introduction

The Millstone Hill (42.6°N, 288.5°E) incoherent scatter radar ran throughout the entire January 20–30, 1993, incoherent scatter coordinated observation day interval, and the data collected from this experiment represent an important resource for studies of the solstice thermosphere/ionosphere system at solar minimum. While most of the interval was geomagnetically quiet, a minor geomagnetic storm occurred on January 25–26, accompanied by an unusual late evening increase in NmF_2 and large increase in hmF_2. This differs from the dusk effect often observed at Millstone Hill during major storms, which consists of an early evening increase in NmF_2 immediately followed by the very low densities associated with a deep trough. A case study of the dusk effect seen during a major storm at Millstone Hill during May 1990 was recently described by *Buonsanto* [1995], who showed it to be due to a combination of mechanisms, including a traveling atmospheric disturbance (TAD), advection of higher-density plasma from lower latitudes, and neutral composition changes. However, it is at present unclear which of these mechanisms operate during other instances of the dusk effect and other storm-related electron density increases. This must be investigated through additional case studies which combine observations and physical models. We investigate in the present study the late evening increase on January 25–26, 1993. In addition to the radar data, we also have measurements of neutral winds collected by the Millstone Hill Fabry-Perot interferometer (FPI) on that night. We are fortunate that model runs are available from the thermosphere ionosphere electrodynamics general circulation model (TIEGCM) with and without inputs from the assimilative mapping of ionospheric electrodynamics (AMIE) procedure, as well as from the coupled thermosphere ionosphere model (CTIM) and the field line interhemispheric plasma (FLIP) model. The availability of runs from these different models affords us with a unique opportunity to assess the relative capabilities of these state-of-the art first-principle models to reproduce a variety of observed parameters at a single location during both quiet and minor storm conditions.

This paper focuses on the interval 1200 UT (0700 LT), January 24 to 1200 UT (0700 LT), January 26, 1993, which included the minor storm. The purpose of the paper is twofold: (1) to compare

[1]Massachusetts Institute of Technology, Haystack Observatory, Westford.
[2]Cooperative Institute for Research in Environmental Sciences, University of Colorado, and Space Environment Center, National Oceanic and Atmospheric Administration, Boulder, Colorado.
[3]High Altitude Observatory, National Center for Atmospheric Research, Boulder, Colorado.
[4]Now at W. B. Hanson Center for Space Sciences, University of Texas at Dallas, Richardson, Texas.
[5]Department of Physics and Astronomy, Dartmouth College, Hanover, New Hampshire.
[6]E. O. Hulburt Center for Space Sciences, Naval Research Laboratory, Washington, D. C.

Paper number 96JA02602.
0148-0227/97/96JA-02602$09.00

results from the four models and the observations to illustrate the current capabilities and shortcomings of the models; and (2) to try to understand the physical mechanisms for the late evening NmF_2 and hmF_2 enhancement in light of all the available data and model results. While numerous other comparisons between global models and data exist [e.g., *Crowley et al.*, 1989b; *Codrescu et al.*, 1992; *Burns et al.*, 1995a b; *Emery et al.*, 1996; *Fesen et al.*, 1989; *Forbes et al.*, 1987; *Hedin et al.*, 1994; *Hernandez and Roble*, 1995; *Szuszczewicz et al.*, 1996; M. V. Codrescu et al., Modeling the *F* layer during specific geomagnetic storms, submitted to *J. Geophys. Res.,* 1996], this is the first such comparison study using four separate first-principle model simulations.

2. Summary of the Solar-Geophysical Conditions Accompanying the Disturbance

The four days January 21–24, 1993, preceding the minor storm interval were geomagnetically quiet, with daily *Ap* varying between 4 and 10. The minor geomagnetic storm of January 25–26 began with a gradual storm commencement observed at eight geomagnetic observatories at times between 0200 and 0900 UT on January 25. The nearest geomagnetic observatory to Millstone Hill is Fredericksburg, Virginia (38.2°N, 282.6°E), where a gradual storm commencement was recorded at 0900 UT, or 0400 LT. *Kp* reached a maximum of 5+ for two 3-hour intervals, and *Ap* was 25 on this day. More details about the solar and geophysical conditions during this minor storm are given in sections 3.3 and 3.4 below where the forcings to the TIEGCM and CTIM models are described.

3. Description of the Data and Models Used

3.1. Incoherent Scatter Radar Experiment and Data Analysis

The Millstone Hill incoherent scatter radar experiment ran from 1232 UT on January 20, 1993, to 0004 UT on January 31, 1993. The experiment included a 0.410-ms pulse length single-pulse mode for *F* region measurements and 0.448-ms pulse length alternating code for the *E* region. During the 25-min experiment cycle, *F* region measurements were taken using both the zenith and steerable antennas, with the steerable antenna pointing north and west at a 45° elevation angle, and pointing up the local magnetic field line. The 0.410-ms pulse gave 61.5-km range resolution, and the alternating code gave 4.2-km range resolution.

Ionospheric F_2 peak densities (NmF_2) and heights (hmF_2) were obtained from spline fits to the 0.410-ms zenith antenna profiles. NmF_2 is calibrated by comparison with foF_2 data obtained with the local Digisonde. The electron temperature (T_e) and ion temperature (T_i) at a constant altitude of 300 km were obtained from similar spline fits to the 0.410-ms zenith T_e and T_i data.

The neutral exospheric temperature (T_{ex}) and atomic oxygen density [O] at 300 km were calculated from the incoherent scatter data by solving the ion thermal energy balance equation [*Bauer et al.*, 1970; *Alcayde et al.*, 1982]. This technique has previously been used by *Salah and Evans* [1973], and *Oliver* [1990] to simultaneously determine T_{ex} and [O] above Millstone Hill. The [O] calculation only works during the daytime when there are sizeable differences between the neutral temperature (T_n), T_i, and T_e.

The ion drift vector at 300 km was obtained from the 0.410-ms data between 250 and 350 km, using measurements taken from the zenith antenna and the steerable antenna pointed to the north and west at 45° elevation angle. The least squares inversion method assumes uniform horizontal velocity above the station but fits a second-degree polynomial to the vertical component. The ion drift vector is decomposed into components antiparallel ($V_{||}$) to the Earth's magnetic field line (*B*), perpendicular to *B* and horizontal eastward ($V_{\perp E}$), and perpendicular to *B* upward and northward ($V_{\perp N}$). The horizontal (magnetic) northward ion drift component (V_n) is also derived for comparison with the neutral meridional wind (U_{mer}). U_{mer} is obtained from $V_{||}$ and a calculation of the velocity of diffusion (V_d) of O^+ along *B* through the neutral atmosphere, using the method of *Salah and Holt* [1974] and the MSIS-86 neutral atmosphere model.

For calculation of U_{mer}, T_{ex}, and [O], the O^+–O collision cross section is required. *Burnside et al.* [1987] analyzed coincident Arecibo incoherent scatter and FPI winds data and concluded that the formula derived by *Dalgarno* [1964] and *Banks* [1966] should be multiplied by a factor F=1.7. A similar study at Millstone Hill [*Sipler et al.*, 1991] gave F=1.9. *Salah* [1993] summarized results to date, suggesting F=1.7 be called the Burnside factor and be adopted as an interim standard for the Coupling, Energetics, and Dynamics of Atmospheric regions (CEDAR) program. Recent work [*Pesnell et al.*, 1993; *Reddy et al.*, 1994; *Davis et al.*, 1995] suggests a smaller *F* value. Use of the smaller cross section recommended by Pesnell et al. results in significantly larger equatorward winds at night when diffusion is more important. For example, the maximum equatorward wind observed on the disturbed night of January 25–26, 1993 was 111 m s^{-1} when the Salah cross section was used, and 147 m s^{-1} when the Pesnell et al. cross section was used. The effect of using the smaller Pesnell et al. cross section on calculations of T_{ex} is very small (<1 K), but it results in an increase of ~50% in [O] obtained from incoherent scatter data during the daytime periods when [O] can be estimated from the ion energy balance equation.

3.2 Fabry-Perot Interferometer Experiment and Data Analysis

The Millstone Hill Observatory Fabry-Perot interferometer operated on the night of January 25–26, 1993, with clear-sky conditions. A slight mechanical misalignment caused the sensitivity of the instrument to be reduced (about 50%), but intensities were high enough that good data were obtained for the period 2253 UT on January 25 to 1120 UT on January 26. Our standard data acquisition observing sequence was used, that is, observations were made at azimuths of 45°, 135°, 225°, and 315°, all at an elevation of 30°. A zenith observation was included and was used as a zero velocity reference for the derivation of line-of-sight winds. Vector winds can be derived from pairs of observations at right angles to each other. We assume that wind variations with longitude are equivalent to local time variations, so that we ignore the NE-SE and NW-SW pairs and use only the NE-NW and SE-SW pairs of observations in our standard analysis, giving us a wind at two different latitudes, to the north and south of the observatory respectively. Latitudinal gradients are observed frequently at Millstone Hill Observatory, and gradients were observed on this night with meridional wind differences up to 100 m s^{-1} at the two latitudes which are separated by about ±3° from Millstone Hill. Since the radar analysis gives winds at the observatory location, our meridional winds from north and south latitudes were linearly interpolated to find the wind overhead. The altitude of peak 630-nm emission was calculated following the method of *Link and Cogger* [1988] and *Sipler et al.* [1991].

3.3. TIEGCM

The TIEGCM, described by *Richmond et al.* [1992], self-consistently calculates electrodynamical interactions in the coupled thermosphere/ionosphere system. The model solves the time-dependent nonlinear primitive equations for momentum, energy,

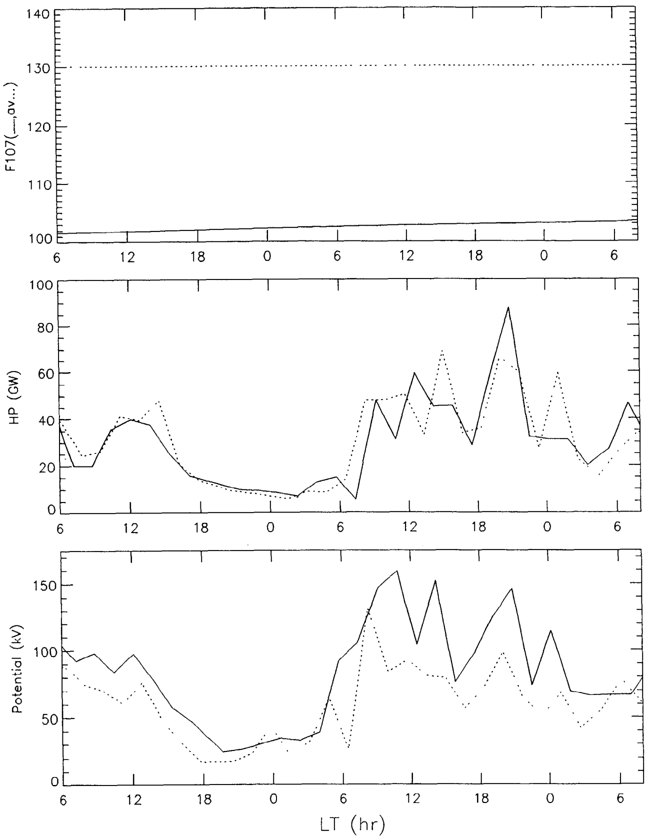

Figure 1. Input values to the TIEGCM using AMIE high latitude inputs from 31 northern hemisphere and 32 southern hemisphere patterns between 1100 UT on January 24 and 1300 UT on January 26, 1993. The *x* axis is the local time at Millstone Hill. (top) Daily 10.7 cm solar flux and the 3-solar rotation average, (middle) hemispheric power in GW, and (bottom) cross-tail potential in kV.

continuity, hydrostatics, current density and the equation of state to obtain predictions of neutral and ionized densities, temperatures, and winds. Chemical species included are N_2, O_2, O, $N(^4S)$, $N(^2D)$, NO, N_2^+, O_2^+, O^+, NO^+ and N^+. The chemical reactions and reaction rates incorporated are identical to those in the field line interhemispheric plasma model described in section 3.5 below. The model has a latitude and longitude resolution of 5°. The vertical dimension is nonuniform and is formulated in pressure levels with 2 grid points per scale height. Typically, the model solves for 25 pressure levels extending from about 97 to 300–500 km with the upper boundary determined by the solar activity level. For this period, the upper boundary was around 450 km.

The required inputs for the TIEGCM are semidiurnal tides at the bottom boundary, O^+ fluxes at the top boundary, solar EUV and UV fluxes parameterized by the daily and 3 solar rotation 10.7 cm solar flux, and a description of the high-latitude energy and momentum sources [e.g., *Roble and Ridley*, 1987]. The prescription of the high-latitude sources are described in the next two sections.

Propagating tidal components are incorporated as perturbations to the lower boundary as described by *Fesen et al.* [1991]. Contributions from the semidiurnal modes (2,2) through (2,6) plus the diurnal (1,1) mode are included [e.g., *Forbes et al.*, 1993].

The solar fluxes during the period were obtained from the National Geophysical Data Center (NGDC). In the model, the fluxes were updated once per day since both the daily and 3-solar rotation fluxes were nearly constant over the campaign as shown in Figure 1a. The daily solar flux varied between 101 and 104, with the 3-solar rotation flux set to 130. These values are close to solar minimum.

Two runs of the TIEGCM were carried out for the January 1993 campaign. The first used the assimilative mapping of ionospheric electrodynamics (AMIE) technique to specify the high-latitude forcings, while the second used only total hemispheric power, cross-polar cap potential, and the east-west component of the interplanetary magnetic field. More information about these two runs is now provided.

3.3.1 TIEGCM with AMIE input. The high latitude inputs needed in the TIEGCM can be specified by the results of the assimilative mapping of ionospheric electrodynamics (AMIE) procedure. The AMIE procedure has been described by *Richmond and Kamide* [1988], and used for various campaign studies [e.g., *Knipp et al.*, 1993]. The high-latitude inputs needed are the electric potential, the auroral electron energy flux, and the mean Maxwellian energy of the auroral electrons. Additional inputs of the cusp and drizzle precipitation are parameterized as a function of the hemispheric power index. The location of the cusp is placed near the dayside convection entry of the AMIE convection patterns, while the polar cap drizzle is placed poleward of the average convection reversal radius.

The AMIE electric potential patterns were first used in the thermosphere general circulation model (TGCM) by *Crowley et al.* [1989a, b] for the period of September 18–19, 1984. The auroral electron energy flux and mean energies are described by *Emery et al.* [1996] and were added to the electric potential results for the March 28–29, 1982, case examined in several thermosphere ionosphere general circulation model (TIGCM) runs [*Lu et al.*, 1995; *Emery et al.*, 1996; *Szuszczewicz et al.*, 1996]. The present study is the first time the AMIE inputs have been used in the TIEGCM model.

The hemispheric power index is used to determine the statistical patterns of auroral electron energy flux [*Fuller-Rowell and Evans*, 1987] as well as the electric potential [*Foster et al.*, 1986]. The Maxwellian mean energy of the electrons is inferred from the ratio of the Hall-to-Pedersen ratio of the *Fuller-Rowell and Evans* [1987] conductance patterns by finding the Maxwellian distribution that produces the same ratio (T. J. Fuller-Rowell, personal communication, 1992).

The hemispheric power is initially estimated from the NOAA 12 satellite and three Defense Meteorological Satellite Program (DMSP) satellites: F8, F10, and F11. The values are binned each UT hour and then converted to a hemispheric power index to determine statistical patterns of the auroral energy flux, mean energy, and electric potential. Conjugacy is assumed, although the error bars on conjugate data are increased by 50%. The resulting AMIE fits of the auroral energy flux uses the measured satellite electron fluxes in addition to estimates from 74 ground magnetometers between 50° and 78° using conductance estimates based on *Ahn* [1983] and converted to auroral energy flux and mean energy using the inverse of the formulas of *Robinson et al.* [1987]. The calculated hemispheric power from these fits is shown in Figure 1b for both hemispheres.

The cross-tail potential drop shown in Figure 1c is calculated from AMIE patterns of electric potential deduced using the initial statistical patterns, ion drift meter (IDM) cross-track drift data from DMSP-F8, F10, and F11, retarding potential analyzer (RPA) along-track drift data from DMSP-F10 and F11, ion drifts from the HF radar at Goose Bay, ion drifts from the incoherent scatter radars at EISCAT and Millstone Hill, and deviation magnetic data from 104 ground magnetometer stations, of which 18 were in the southern hemisphere. The magnetometer data required conductance esti-

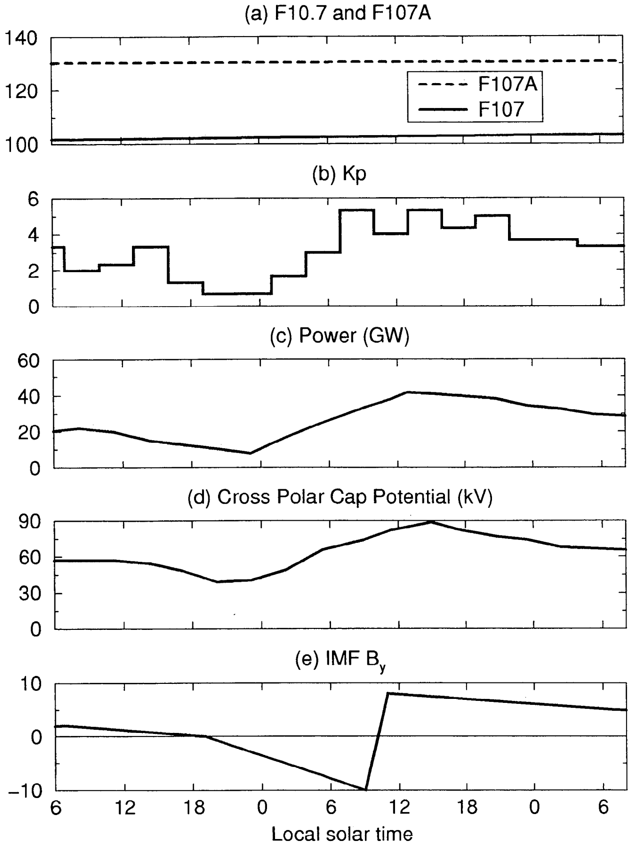

Figure 2. Input values to the TIEGCM without AMIE on January 24–26, 1993. (a) Daily 10.7-cm solar flux and the 3-solar rotation average, (b) geomagnetic *Kp* index, (c) hemispheric power in GW, (d) cross-tail potential in kV, and (e) Interplanetary magnetic field y component. The *x* axis is the local time at Millstone Hill.

mates that were found in conjunction with the auroral parameters described above. The ground magnetometer coverage was not very even, with great data gaps over oceans and Russia. That is why the data times were selected to coincide with DMSP passes with ion drift data in each hemisphere, and why ±35 min (or 70 min) of data were averaged into each calculation.

The final AMIE patterns were converted to the TIEGCM grid and linearly interpolated between the UT times of each pattern. Because of conjugacy, the auroral inputs were updated in each hemisphere by duplicating whatever pattern was available in the opposite hemisphere. The electric potential patterns were specific to each hemisphere because of differing IMF By effects. The potential drops in Figure 1c are similar in both hemispheres and give rise to similar structures in the Joule heating. The Joule heating events should give rise to gravity waves which may or may not be detected at Millstone Hill depending on the location of the heating with respect to Millstone.

3.3.2. TIEGCM without AMIE input. In the TIEGCM run which does not incorporate the AMIE technique to represent the high-latitude energy and momentum sources, the cross-polar-cap potential (CCP), the total hemispheric power (HP), and the east-west component of the interplanetary magnetic field (B_y) are used to parameterize the effects of auroral processes. The components of the interplanetary magnetic field were obtained from the National Space Science Data Center (NSSDC). The NSSDC data were used to specify B_y at 12-hour intervals during the January 1993 campaign; the sparseness of the data precluded more detailed information. The CCP and HP were calculated from the *Kp* index which was obtained from the NGDC for the observation period. Time histories of the *Kp* index, HP, CCP, and B_y for the campaign period are shown in Figure 2. While the actual *Kp* values (constant for each 3-hour interval) are shown in Figure 2, *Kp* was assumed to vary smoothly between points at the middle of each 3-hour interval. The relation between CCP and *Kp* was parameterized as $CCP = 29 + 11Kp$ (P. H. Reiff, personal communication, 1985). The result was a set of CCP values at 3-hour intervals over the campaign. A three-point smoothing was then done using a boxcar average; thus the final set of CCP values represents a smoothing over 6 hours. Similarly, the relation between HP and *Kp* was expressed as $HP = -2.78 + 9.33Kp$ [*Maeda et al.*, 1989]. The resulting set of 3-hour HP values was smoothed over 5 points so that the final set of HP values was smoothed over 12 hours. The empirical convection model of *Heelis et al.* [1982] is used for calculations of ion drag and Joule heating which are updated at each time step.

3.4. CTIM

The coupled thermosphere ionosphere model (CTIM) has been presented in previous publications by *Fuller-Rowell and Rees* [1980, 1983] and *Fuller-Rowell et al.* [1987], and used extensively over the last 15 years.

The thermospheric code simulates the time-dependent structure of the wind vector, temperature, and density of the neutral thermosphere by numerically solving the non-linear primitive equations of momentum, energy, and continuity. The global atmosphere is divided into a series of elements in geographic latitude, longitude, and pressure. Each grid point rotates with Earth to define a noninertial frame of reference in a spherical polar coordinate system. The momentum equation is nonlinear, and the solution describes the horizontal and vertical advection, curvature and Coriolis effects, pressure gradients, horizontal and vertical viscosity, and ion drag. The nonlinear energy equation is solved self-consistently with the momentum equation; it includes three-dimensional advection, horizontal and vertical heat conduction by both molecular and turbulent diffusion, heating by solar UV and EUV radiation, cooling by infrared radiation, and Joule heating. Time-dependent major species composition equations are solved including the evolution of O, O_2, and N_2, under chemistry, transport and mutual diffusion [*Fuller-Rowell et al.*, 1994]. The time-dependent variables of southward and eastward wind, total energy density, and concentrations of O, O_2, and N_2 are evaluated at each grid point by an explicit, time-stepping numerical technique.

The equations for the neutral thermosphere are solved self-consistently with a high-latitude and midlatitude ionospheric convection model [*Quegan et al.*, 1982]. In the version of CTIM used here, the ionosphere is computed self-consistently with the thermosphere poleward of 23 deg latitude in both hemispheres. The empirical ionospheric model of *Chiu* [1975] is used at equatorial latitudes. In this coupled model the ionospheric Lagrangian frame has been modified to be more compatible with the Eulerian frame by the use of a semi-Lagrangian technique [*Fuller-Rowell et al.*, 1987]. Transport under the influence of the magnetospheric electric field is explicitly treated, assuming **ExB** drifts and collisions with the neutral particles. The densities of atomic ions H^+ and O^+ and the ion temperature are evaluated over the height range from 100 to 10,000 km, including horizontal transport, vertical diffusion and the ion-ion and ion-neutral chemical processes. Below 400 km the additional contribution from the molecular ion species N_2^+, O_2^+, and NO^+ and the atomic ion N^+ are included. The ion temperature is calculated under the assumption of thermal balance between heat

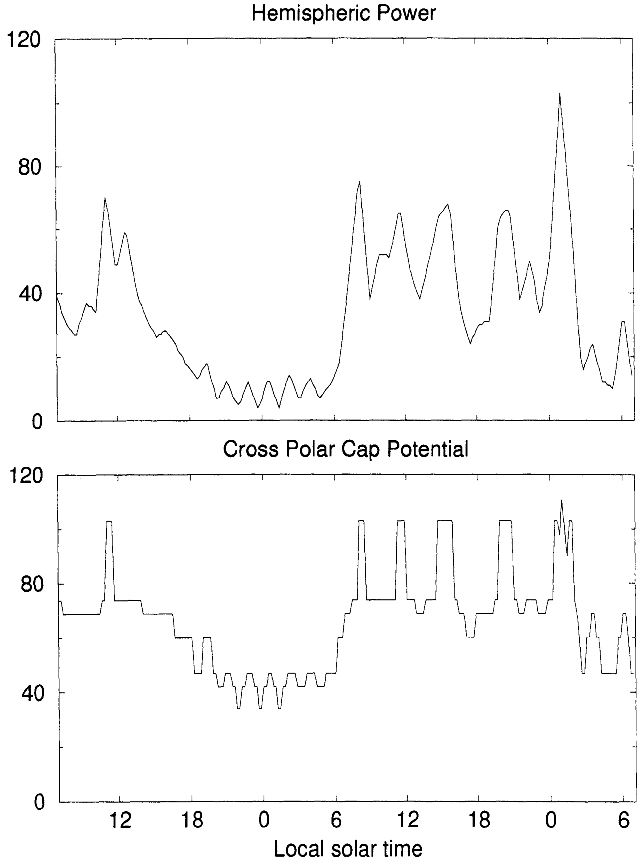

Figure 3. Inputs to CTIM on January 24–26, 1993. (top) Hemispheric power (GW), derived from TIROS/NOAA auroral particle measurements. (bottom) Cross polar cap potential drop (kV) derived from the statistical electric field patterns of *Foster et al.* [1986]. The electric fields have been increased by 30% to account for effects of electric field variability on the high-latitude Joule heating rate.

gained from the electron gas and from ion-neutral frictional heating, and heat lost to the neutral gas.

The magnetospheric input to the model can be specified in several ways. For the simulations described here, we used the statistical patterns of auroral precipitation and electric field described by *Fuller-Rowell and Evans* [1987] and *Foster et al.* [1986], respectively. The hemispheric power index (HP), derived from TIROS/NOAA auroral particle measurements, is used to determine the sequence of statistical input patterns for this specific period. The relationship between HP and *Kp* can be found in the work of *Foster et al.* [1986].

The hemispheric power index and cross polar cap potential for January 24–26, 1993, are shown in Figure 3. The statistical patterns used as input are somewhat broadened in latitude compared with instantaneous observations of auroral precipitation and *E* fields. Furthermore, the use of the statistical patterns means using average *E* field values for the computation of Joule heating, which may reduce the magnetospheric energy deposited at high latitudes by 30% [*Codrescu et al.*, 1995]. For these reasons, the electric fields used in the simulations described in this paper are increased above the original model values of [*Foster et al.*, 1986], by 30%.

3.5 FLIP model

The field line interhemispheric plasma model (FLIP) solves coupled ion continuity and momentum equations, electron and ion energy equations, and photoelectron transport equations along the entire L=3 flux tube over Millstone Hill starting above 80 km in each hemisphere [*Richards et al.*, 1994a, b]. The model has been tested and validated with many different data sets during the past 10 years. In this run, the FLIP model calculates the densities and field aligned diffusive velocities of major and minor ions as described by *Craven et al.* [1995] simultaneously with many other quantities [*Torr et al.*, 1990]. Solar EUV fluxes are calculated using the EUVAC model [*Richards et al.*, 1994c]. Momentum forcing is provided by calculating the equivalent meridional wind as needed to fit the F_2 peak height (hmF_2) at each model time step using the algorithm of *Richards* [1991]. In the northern hemisphere, FLIP uses the hmF_2 measured by the Millstone Hill radar; in the southern hemisphere the values of hmF_2 predicted by the International Reference Ionosphere (IRI) [*Bilitza*, 1986] are used given the lack of simultaneous measurements. The model can also run with any input meridional (equivalent) winds; results based on different wind assumptions are discussed by D. J. Melendez-Alvira et al. (unpublished manuscript, 1996).

The model ran in a storm-mode where 3-hourly *Kp* values are input to the MSIS-86 model in order to simulate the effects of magnetic activity on the thermosphere. Both MSIS and EUVAC require specification of the daily $F10.7$ index to determine short-term variations and the 81-day centered average $F10.7$ to determine long-term variations. Photoelectron energy fluxes are calculated with a modified two-stream transport algorithm [*Young et al.*, 1980]. An adjustable parameter in the model is the fraction of the energy of the escape photoelectron flux that is trapped in the plasmasphere and prevented from reaching the ionosphere. This parameter represents the phenomenological loss of photoelectrons due to pitch angle and energy scattering in the plasmasphere [*Lejeune and Wormser*, 1976; *Mantas et al.*, 1978; *Khazanov and Liemohn*, 1995]. In this run 20% of the escape photoelectron energy flux is trapped continuously although the photoelectron flux varies in time and altitude. The trapped energy is redeposited as an electron heat flux that ultimately heats ionospheric thermal electrons. The choice of 20% is conservative and consistent with photoelectron transparencies calculated by Khazanov and Liemohn and with trapping factors needed to model measured ion temperatures by *Newberry et al.* [1989].

4. Results and Discussion

Figure 4 shows the exospheric temperature T_{ex} determined from the radar data and heat balance calculation, compared with T_{ex} given by the MSIS-86 model, and neutral temperature (T_n) at 300 km given by the CTIM, the AMIE TIEGCM, and the no AMIE TIEGCM runs. The difference between T_n at 300 km and T_{ex} in the MSIS-86 model is small (~ 10 K or less). The radar data agree quite well with MSIS-86, however the CTIM and TIEGCM model runs give temperatures ~100 K smaller. This is apparently due to an underestimate of the high latitude Joule heating in the models. A 30% increase in high latitude electric fields was included in CTIM to account for effects of electric field variability on the Joule heating rate [*Codrescu et al.*, 1995], but even larger electric fields would be needed to give agreement with the data. While the AMIE TIEGCM electric fields are most accurate due to the large amount of data used in deriving them, the Joule heating rate does not include a correction for electric field variability. Such a correction would improve agreement with the radar data and MSIS model T_n.

Figure 5 shows the neutral atomic oxygen density [O] at 300 km obtained from the same radar data and heat balance calculation, compared with [O] from MSIS-86 and the CTIM, AMIE TIEGCM, and no AMIE TIEGCM model runs. The estimated uncertainty in

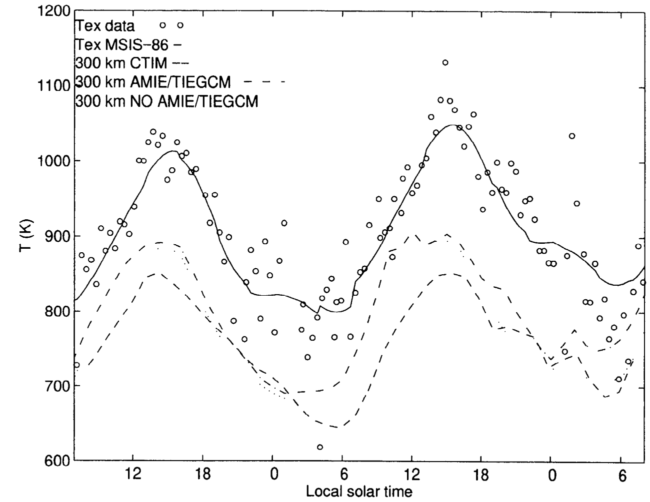

Figure 4. Exospheric temperature on January 24–26, 1993, derived from Millstone Hill incoherent scatter radar data using a heat balance calculation (circles), and given by the MSIS-86 model (solid line). Neutral temperature at 300 km altitude given by CTIM (dashed curve), the AMIE TIEGCM (dot-dashed curve), and the no AMIE TIEGCM (dotted curve).

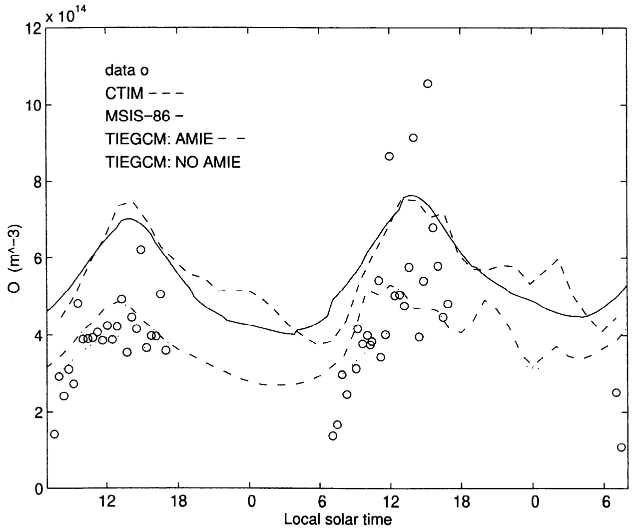

Figure 5. Atomic oxygen density at 300 km altitude on January 24–26, 1993, derived from Millstone Hill incoherent scatter radar data using a heat balance calculation (circles), and given by the MSIS-86 model (solid line), CTIM (dashed curve), the AMIE TIEGCM (dot-dashed curve), and the no AMIE TIEGCM (dotted curve). Calculations used the O^+–O collision cross section recommended by *Salah* [1993].

MSIS-86 [O] is 15–30% [*Hedin*, 1987]. The heat balance calculation used the O^+–O collision cross section recommended by *Salah* [1993]. This cross section includes a 1.7 multiplicative factor times the cross section of [*Dalgarno*, 1964; *Banks*, 1966]. The [O] obtained from this heat balance calculation using the radar data are generally smaller than the MSIS-86 model [O]. However, if the smaller O^+–O collision cross section recommended by *Pesnell et al.* [1993] were used, the derived [O] would increase by ~ 50%, giving good agreement with the MSIS-86 model. The Pesnell et al. cross section includes a factor of 1.3 times the cross section of *Dalgarno* [1964] and *Banks* [1966]. The CTIM [O] also agrees well with MSIS, but [O] from the two TIEGCM runs are lower, in better agreement with the results of the radar heat balance calculation using the Salah et al. O^+–O collision cross section.

Figure 6 shows the electron temperature (T_e) and ion temperature (T_i) as measured by the incoherent scatter radar, compared with results from the FLIP model, the AMIE TIEGCM and no AMIE TIEGCM model runs. The FLIP model agrees well with the observed T_i, and reproduces many features of the T_e variation as well. One feature it misses, however, is the large T_e enhancement on the night of January 24–25. Such large nighttime T_e enhancements are frequently observed in winter at Millstone Hill [*Garner et al.*, 1994]. They are apparently associated with heating due to photoelectrons originating in the sun-lit conjugate hemisphere. T_e and T_i from both TIEGCM model runs generally underestimate the data. This may be due to the large values of NmF_2 in the TIEGCM (shown below), since the electron cooling rate is proportional to the electron density. The ion temperature is determined by a balance between heating due to collisions with the electrons and cooling via collisions with the neutrals (heat balance). Thus the low TIEGCM T_i is a consequence of the low TIEGCM T_n and T_e.

Figure 7 shows the horizontal neutral wind in the magnetic meridian plane (U_{mer}), positive northward, given by the incoherent scatter radar, the Fabry-Perot interferometer, and the CTIM, AMIE TIEGCM, and no AMIE TIEGCM runs. The radar winds as well as the CTIM and TIEGCM winds were calculated at a height of 300 km. FPI wind measurements were not available for the night of January 24–25. For the FPI winds on the night of January 25–26 our calculations of the altitude of peak 630-nm emission gave values varying between 257 and 294 km over the course of the night. The lower altitude may explain why the FPI winds are generally smaller in magnitude compared to the radar winds. The winds derived from the radar data are generally more southward than the model winds over the 2-day interval. As the thermospheric circulation is set up by pressure gradients originating in high-latitude Joule and particle heating, the underestimate of the high-latitude Joule heating discussed earlier could be the cause of this difference between the radar and model winds. *Hagan* [1993] calculated average quiet time wind patterns at 300 km altitude from Millstone Hill radar data and found that the meridional winds at solar minimum had a strong equatorward component, in agreement with the present radar results.

The night of January 25–26 was characterized by recurrent equatorward surges in the neutral wind, followed by abatements. This

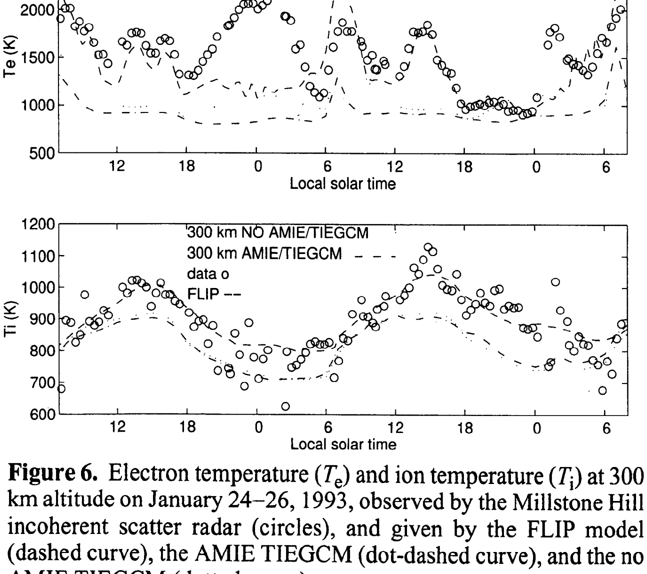

Figure 6. Electron temperature (T_e) and ion temperature (T_i) at 300 km altitude on January 24–26, 1993, observed by the Millstone Hill incoherent scatter radar (circles), and given by the FLIP model (dashed curve), the AMIE TIEGCM (dot-dashed curve), and the no AMIE TIEGCM (dotted curve).

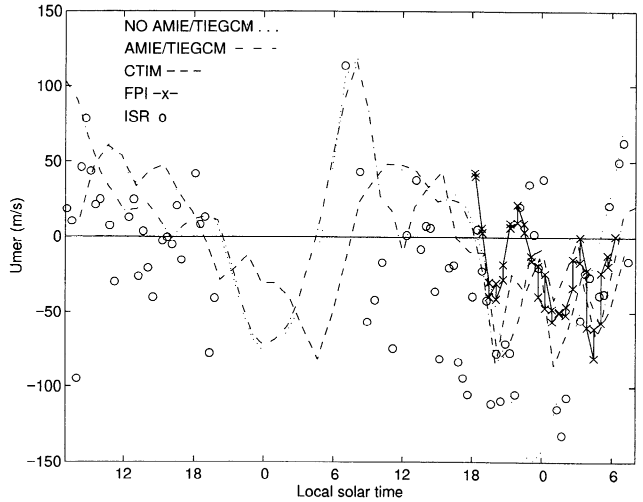

Figure 7. Meridional neutral wind (U_{mer}) on January 24–26, 1993, observed by the Millstone Hill Fabry-Perot interferometer (crosses) and observed at 300 km altitude by the Millstone Hill incoherent scatter radar (circles), compared with U_{mer} at 300 km given by CTIM (dashed curve), the AMIE TIEGCM (dot-dashed curve), and the no AMIE TIEGCM (dotted curve).

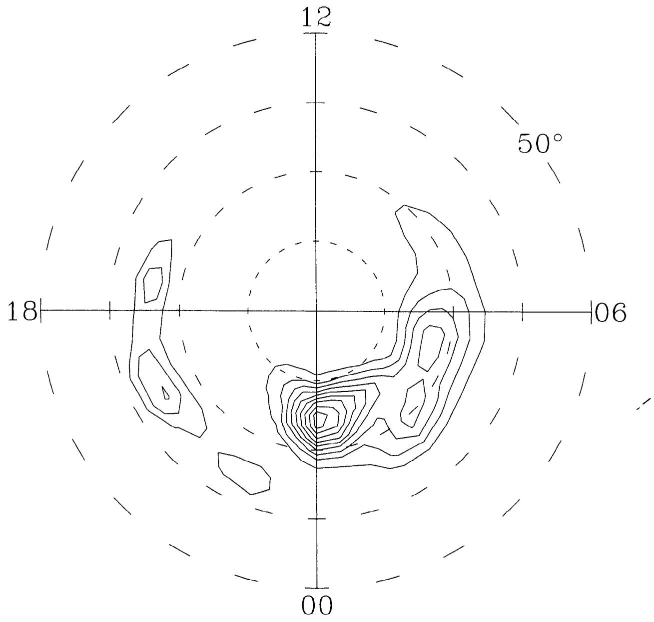

Figure 8. Simple Joule heating (330.6 GW) from AMIE in the northern hemisphere at 0150 UT on January 26, 1993 (2050 LT on January 25 at Millstone Hill) as a function of magnetic latitude and magnetic local time. The large heating near 75 deg magnetic latitude and 0000 MLT is the source region of the gravity wave launched around 0000 UT and seen at Millstone Hill shortly afterward as increases in the equatorward wind and the hmF_2.

pattern is seen in both the radar and FPI wind data, and is reproduced by CTIM and the AMIE TIEGCM. The equatorward surges are clearly associated with the passage of traveling atmospheric disturbances seen in both the AMIE TIEGCM and CTIM results. These surges are not seen in the no AMIE TIEGCM results because of the considerable smoothing of the model inputs (Figure 2).

Figure 8 shows the simple Joule heating at 0150 UT on January 26 (2050 LT on January 25 at Millstone Hill) from AMIE. This is related to the square of the electric field multiplied by the Pedersen conductance, where the effects of the neutral wind are ignored. The neutral winds generally decrease the magnitude of the Joule heating by about 30% [*Lu et al.*, 1995] but do not usually move the regions of maximum Joule heating, which are a source region for gravity waves and TADs. Figure 8 shows strong Joule heating near 0000 MLT, which began earlier around 0000 UT and ended before 0300 UT. A gravity wave is seen in the AMIE TIEGCM propagating to the equator in about 2 hours along the 75°W meridian near Millstone Hill with maximum upward vertical velocities around 300 km occurring between 0000 and 0300 UT and between 62° and 72° geographic latitude. This corresponds to a region between 72° and 82° magnetic latitude and around 2130 MLT at 0150 UT. Comparison with Figure 8 shows that the source region for the gravity wave seen at 75°W is the western edge of the large heating near 0000 MLT. The direct effects of the gravity wave at Millstone in the AMIE TIEGCM results are increases in the equatorward wind between 0100–0200 UT (2000–2100 LT in Figure 7), and increases in the hmF_2 between 0100–0300 UT (2000–2200 LT in Figure 10 discussed later).

Figure 9 shows the vertical ion drift velocity as seen in incoherent scatter radar zenith antenna measurements from midafternoon through the evening of January 25. Figure 9 reveals a complicated pattern of updrafts and downflows caused by the neutral winds and electric fields present during this period. Increases in NmF_2 and hmF_2 (discussed below) appear to be related to the strong downward fluxes near 1800, 1945, and 2230 LT. The magnitude of the large downward flux at 1800 LT is also partly the normal sunset downward flux described by *Evans* [1975]. Upward drifts from low altitudes at the times of downward fluxes from the topside result in a convergence of ionization into the F_2 peak region.

Figure 10 shows NmF_2 and hmF_2 for the 2-day interval. The radar data are shown, together with results from the FLIP model, CTIM, AMIE TIEGCM, and no AMIE TIEGCM runs. The FLIP model automatically adjusts itself to match the observed hmF_2. NmF_2 from the FLIP model is a little low compared to the data. This could be due to an inadequate downward H^+ flux, or an underestimate of the $[O]/[N_2]$ ratio by the MSIS-86 model. CTIM agrees well with the NmF_2 data, though hmF_2 is a little low. AMIE TIEGCM produces the largest values of NmF_2, and hmF_2 is low. This is apparently associated with the inadequate Joule heating rate and with the low neutral temperature shown in Figure 4. An increase in the high-latitude Joule heating would modify the thermospheric circulation resulting in increases in N_2 and O_2 density above Millstone Hill. This would increase the O^+ recombination rate, decreasing the AMIE TIEGCM peak electron density (NmF_2) to agree better with the observations, but would result in poorer agreement between CTIM and the data. Since the F_2 peak lies near the level where recombination and diffusion are of approximately equal importance [*Rishbeth*, 1967], a larger recombination rate would also result in a higher hmF_2, again in better agreement with the radar data. NmF_2 from the no AMIE TIEGCM agrees better with the NmF_2 data, in spite of a low T_n. This is apparently a consequence of the lower atomic oxygen density in the no AMIE TIEGCM compared to the AMIE TIEGCM (Figure 5).

The large downdrafts of vertical ion velocity on the evening of January 25 shown in Figure 9 at upper altitudes appear to be correlated with strong updrafts below 250 km. The convergences around 1800, 1945, and 2230 LT appear to lead to increases in the hmF_2 in Figure 10, with the largest sustained increase seen around 2230 LT. There are corresponding increases at these times in the N_e contours shown in Figure 11, which are again most noticeable in NmF_2 in Figure 10 around 2230 LT. The increases in NmF_2 are most likely the combined result of lower loss rates from having the layer lifted up, an increase in the downward O^+ flux, and a convergence of ion-

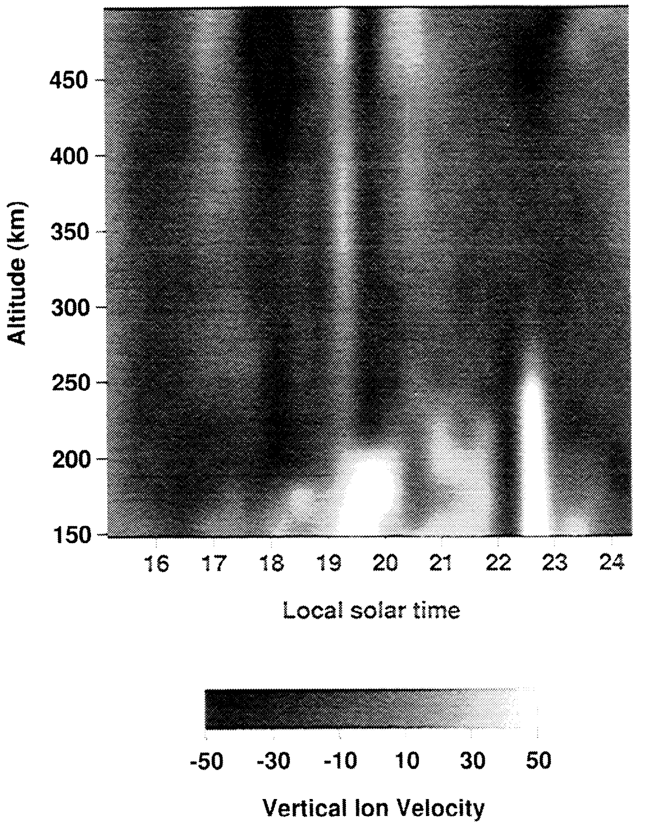

Figure 9. Vertical ion velocity versus altitude and time observed by the Millstone Hill incoherent scatter radar from the midafternoon through the evening of January 25, 1993, showing updrafts and downdrafts associated with the passage of traveling atmospheric disturbances.

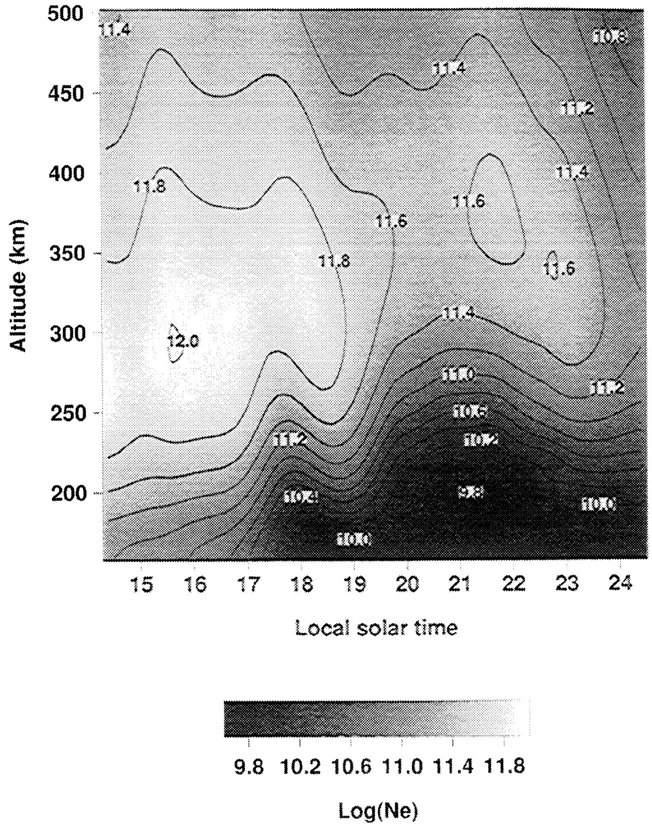

Figure 11. Log (electron density) versus altitude and time observed by the Millstone Hill incoherent scatter radar from the midafternoon through the evening of January 25, 1993, showing an enhancement in $NmF2$ near 2200 LT coincident with a large increase in $hmF2$.

ization into the F_2 peak region. Neither the CTIM nor the TIEGCM reproduce the large hmF_2 increase, though AMIE TIEGCM gives a small increase.

The O^+ flux is a product of the electron density in Figure 11 and the vertical ion drift in Figure 9. A test AMIE TIEGCM run was made between 2100–2400 LT on January 25 (0200–0500 UT on January 26) where the downward O^+ nighttime flux was increased worldwide by a factor of 10 to a peak of -1.5×10^9 cm^{-2}s^{-1} at 2230 LT (0330 UT) consistent with the flux measured around 450 km by the Millstone radar. There was an increase in the NmF_2 at 2330 LT, one hour after the maximum downward flux, which was a a little over a factor of 2 increase in NmF_2 compared to the value at 2130 LT, and a little over a factor of 3 increase in NmF_2 at 2400 LT compared to the standard run which had a constant nighttime downward O^+ flux of -1.5×10^8 cm^{-2}s^{-1}. With the large increase in N_e was a corresponding decrease of 150 K in T_e at 2400 LT. The hmF_2 decreased before by 35 km in this 3-hour period, but in the test run, increased by 13 km in the first hour, and then decreased by 43 km to be within 5 km of hmF_2 in the standard run. There were only small changes in the other parameters with this transitory increase in the O^+ flux at night.

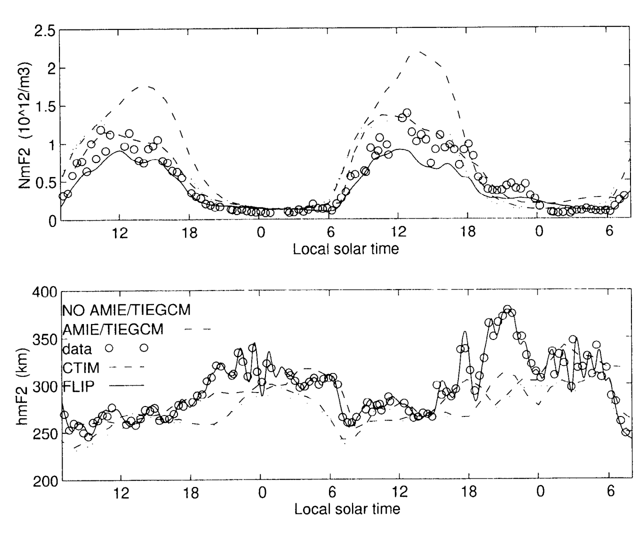

Figure 10. Ionospheric $F2$ peak electron density (NmF_2) and peak height (hmF_2) on January 24–26, 1993, observed by the Millstone Hill incoherent scatter radar (circles), and given by the FLIP model (solid curve), CTIM (dashed curve), the AMIE TIEGCM (dot-dashed curve), and the no AMIE TIEGCM (dotted curve).

To further aid our interpretation of the variations of NmF_2 and hmF_2, we show in the bottom panel of Figure 12 a comparison of U_{mer} with the northward (horizontal) ion drift velocity (V_n) observed by the incoherent scatter radar. The top panel shows the time constant for ion drag, which is the inverse of the neutral-ion collision frequency, calculated using the observed electron density at 300 km and the MSIS-86 model. A short time constant means the ions can effectively accelerate the neutrals through collisions, so that the neutral wind tends to follow the ion motion. The ion drag time constant increases greatly after midnight due to the sharp decrease in electron density (Figure 10). On January 24 the winds and ion drifts are closely coupled, but major differences are seen between U_{mer} and V_n during the minor storm interval (January 25–26) due to rapid changes in electric fields and neutral winds. In par-

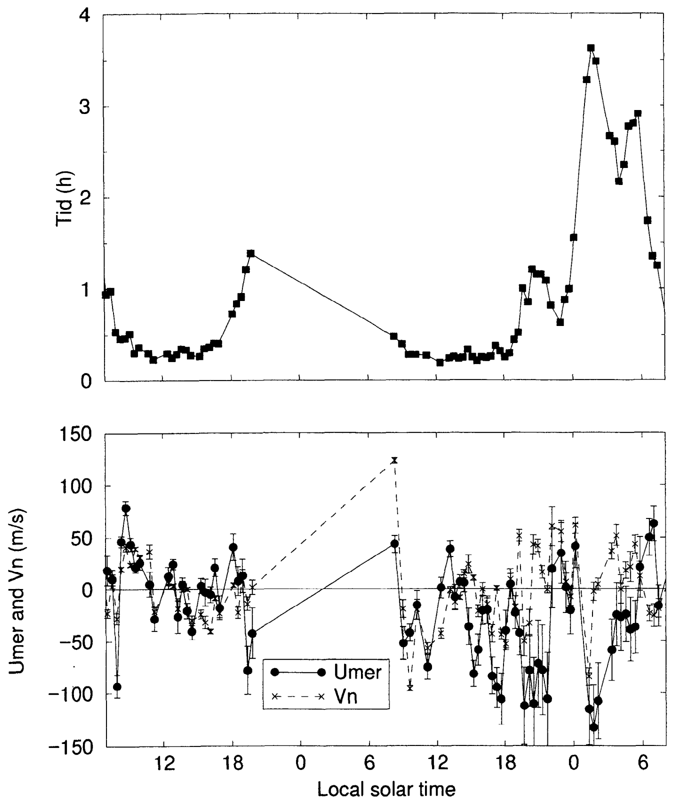

Figure 12. Millstone Hill, January 24–26, 1993. (top) Time constant for ion drag, which is the inverse of the neutral-ion collision frequency, calculated using the observed electron density and the MSIS-86 model. (bottom) Neutral wind (U_{mer}) and ion drift (V_n), both in the magnetic meridian plane, horizontal, and positive northward.

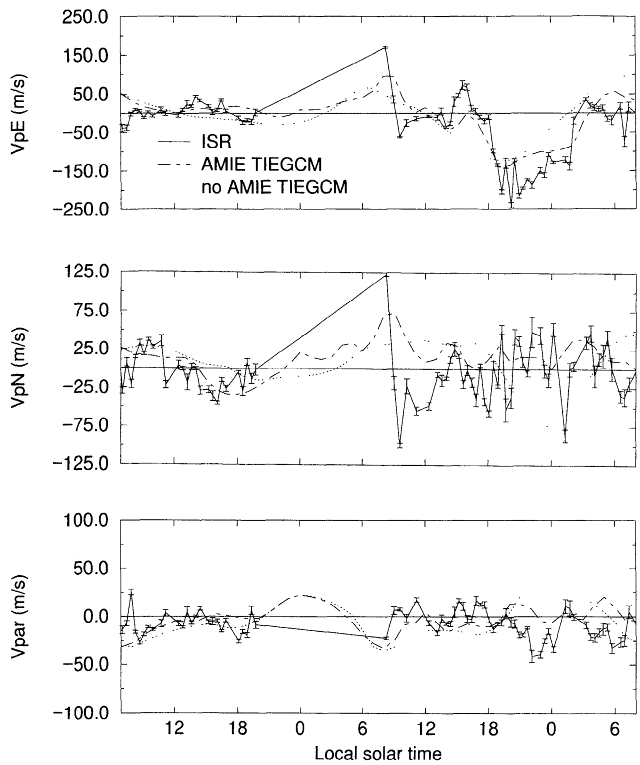

Figure 13. Components of the ion drift vector at 300 km altitude above Millstone Hill on January 24–26, 1993. (top) $V_{\perp E}$, perpendicular to the Earth's magnetic field, positive eastward. (middle) $V_{\perp N}$, perpendicular to the Earth's magnetic field, positive northward. (bottom) $V_{\parallel}$, antiparallel to the Earth's magnetic field, positive upward. Millstone Hill incoherent scatter radar data (solid line) are compared with results from the AMIE TIEGCM (dashed line) and the no AMIE TIEGCM (dotted line).

ticular, during the strong equatorward wind surge between 1900 and 2200 LT, the ion drift is predominantly northward, due to the penetration of magnetospheric electric fields to the latitude of Millstone Hill.

Figure 13 shows the ion drift components derived from the three-position radar measurements and the AMIE TIEGCM and no AMIE TIEGCM. The top panel shows $V_{\perp E}$, the component perpendicular to the Earth's magnetic field and eastward. During the minor storm interval, this component shows a strong westward drift until 0200 LT, illustrating that the magnetospheric convection pattern has expanded to the latitude of Millstone Hill. The middle panel shows $V_{\perp N}$, the component perpendicular to the Earth's magnetic field and northward. This component is primarily responsible for the northward V_n shown in Figure 11 between 1900 and 2200 LT on January 25. The upward component of the perpendicular northward ion drift and the southward neutral wind surge combine to increase hmF_2 as shown in Figures 10–11. During a major storm in May 1990, *Buonsanto* [1995] showed that a northward ion drift brought higher density lower latitude plasma into the field of view of the Millstone radar, contributing to a large evening NmF_2 increase (dusk effect). This mechanism has previously been described by *Foster* [1993]. Examination of the electron density data to the north and south and above the station on the evening of January 25 does show a large dropoff in density to the north of Millstone Hill. However, approximately the same electron density was seen above the station and at a location one degree of latitude to the south. So it appears that during the present event, north-south gradients in electron density may not have contributed to the evening NmF_2 increase seen above Millstone Hill.

The AMIE TIEGCM shows a northward $V_{\perp N}$ between 1900 and 2200 LT in agreement with the data, but the no AMIE TIEGCM does not. The agreement between AMIE and the data might be expected since the Millstone Hill data were included in the AMIE analysis. The bottom panel of Figure 13 shows $V_{\parallel}$, the component of the ion drift velocity upward along the Earth's magnetic field. This component is small and unexpectedly downward during the equatorward wind surge. While the neutral wind tends to lift the plasma up the field line, this effect is overcome by a large downwards diffusion velocity. $V_{\parallel}$ becomes strongly negative (downward) when the neutral wind turns northward at 2200 LT.

It appears from the preceding that the large rise in hmF_2 and the NmF_2 increase above Millstone Hill on the evening of January 25, 1993, was a complex local event, beyond the capabilities of the best current large-scale first-principle models to easily reproduce. The rise in peak height was much larger than the normal rise associated with the turn-off of production and consequent increased decay at lower levels. The perpendicular northward ion drift and southward wind surge clearly produced an uplifting effect. The increase in peak density is partly explained by the large hmF_2 rise, which decreased markedly the O^+ recombination rate at the F_2 peak. However, compressional effects of traveling atmospheric disturbances and increased downward fluxes of ionization appear to have contributed to it. The possible role of neutral composition changes associated with the geomagnetic activity [e.g., *Burns et al.*, 1991] has not been possible to assess since there are no observations of $[N_2]$ or $[O_2]$ and neither the TIEGCM nor CTIM reproduced the NmF_2 increase.

5. Conclusions

In this paper we have compared results from four first principle model runs with Millstone Hill incoherent scatter radar and Fabry-Perot interferometer data collected during January 24–26, 1993. This interval included a minor storm with a late evening increase in NmF_2 accompanied by a large increase in hmF_2. We report here the first results from the NCAR TIEGCM run with input from the AMIE technique, as well as results from the no AMIE TIEGCM, CTIM, and the FLIP model.

The TIEGCM and CTIM underestimated the neutral temperature due to an inadequate Joule heating rate. While CTIM included a 30% increase in high-latitude electric fields to account for effects of E field variability [*Codrescu et al.*, 1995], this increase is not sufficient to reproduce the observed T_n. No such increase in high-latitude heating was applied to the TIEGCM. A larger high-latitude Joule heating rate would modify the thermospheric circulation, which could increase the N_2 and O_2 density above Millstone Hill resulting in a larger O^+ recombination rate. This would decrease the AMIE TIEGCM NmF_2 to agree better with the observations, but would result in poorer agreement between CTIM and the data. Good agreement was found between [O] given by the MSIS-86 model and the radar data provided an O^+–O collision frequency factor of 1.3 was used. Best agreement with observed T_e and T_i was given by the FLIP model, although it could not reproduce the large nighttime enhancement in T_e on January 24–25. Throughout most of the 2-day interval, the observed neutral winds are more equatorward or less poleward, compared to the winds given by the TIEGCM or CTIM. This may be due to the inadequate high-latitude heating rate in the models.

During the minor storm on the evening of January 25, the observed and model neutral winds show alternating equatorward surges and abatements which are accompanied by strong updrafts and downdrafts in O^+ ion velocity seen by the incoherent scatter radar. Traveling atmospheric disturbances (TADs) are seen in the CTIM and TIEGCM at these times. Neither CTIM nor the TIEGCM is able to reproduce the large hmF_2 increase and the NmF_2 increase (2130–2300 LT), although the AMIE TIEGCM does show a small increase in $hmF2$. This increase in hmF_2 appears to be associated with a perpendicular northward ion drift due to an electric field of magnetospheric origin, coincident with a strong southward neutral wind surge at a time when the electron density at lower altitudes is decaying rapidly due to lack of production. The best explanation for the NmF_2 increase appears to be a downward flux of O^+ ions coincident with a convergence of ionization into the F_2 peak due to the passage of the TADs.

Acknowledgments. We are grateful to P. Erickson for his assistance in interpretation of the incoherent scatter radar autocorrelation functions during times of rapid changes in line-of-sight ion drift velocities. Millstone Hill radar data were acquired and analyzed under the support of National Science Foundation (NSF) cooperative agreements ATM-91-02445 and ATM-94-08609 to the Massachusetts Institute of Technology. The CTIM modeling effort was supported in part by NASA grant NAGW-3530 to the University of Colorado. The efforts of C.G.F. were supported by NSF grant ATM 94-95177 and by NASA through grant NAGW2656. The NSF grant was from the CEDAR program. Computing time was provided by the National Center for Atmospheric Research (NCAR) which is also sponsored by NSF. The AMIE calculation owes thanks to many data providers. Electron precipitation measurements and estimates of the hemispheric power were provided by Fred Rich and Bill Denig of Phillips Lab for the DMSP satellites, and by Dave Evans of the Space Environment Center for NOAA 12. The Goose Bay HF measurements were provided by Michael Ruohoniemi of the Applied Physics Laboratory to the CEDAR Data Base at NCAR. The Goose Bay HF radar is operated by the Applied Physics Laboratory of the Johns Hopkins University with support from NSF. EISCAT ion drifts were provided by T. S. Virdi of Aberystwyth, Wales. The EISCAT Scientific Association is supported by Centre National de la Recherche Scientifique of France, Suomen Akatemia of Finland, Max-Planck-Gesellschaft of Germany, National Institute for Polar Research of Japan, Norges Forskningsrad of Norway, Naturvetenskapliga Forsknigsradet of Sweden, and the Particle Physics and Astronomy Research Council of the United Kingdom. DMSP IDM and RPA drifts were provided by Marc Hairston of the University of Texas at Dallas. Ground magnetometer data were provided by Les Morris of the National Geophysical Data Center in Colorado, Eigil Friis-Christensen of the Meteorologisk Institut in Denmark, Mark Engebretson of Augsburg College in Minnesota, Terry Hughes of the National Research Council of Canada, David Milling of the University of York in the United Kingdom, Toby Clark of the British Geological Survey, and Carol Maclennan of AT&T Bell Laboratories in New Jersey.

The Editor thanks Q. H. Zhou for his assistance in evaluating this paper.

References

Ahn, B.-H., R. M. Robinson, Y. Kamide, and S.-I. Akasofu, Electric conductivities, electric fields and auroral particle energy injection rate in the auroral ionosphere and their empirical relations to the horizontal magnetic disturbances, *Planet. Space Sci., 31*, 641–653, 1983.

Alcayde, D., J. Fontanari, and P. Bauer, High latitude neutral atmosphere temperature and concentration measurements from the first Eiscat incoherent scatter observations, *Ann. Geophys., 38*, 473–480, 1982.

Banks, P., Collision frequencies and energy transfer: Ions, *Planet. Space. Sci., 14*, 1105–1122, 1966.

Bauer, P., P. Waldteufel, and D. Alcayde, Diurnal variations of the atomic oxygen density and temperature determined from incoherent scatter measurements in the ionospheric *F* region, *J. Geophys. Res., 75*, 4825–4832, 1970.

Bilitza, D., International reference ionosphere: Recent developments, *Radio Sci., 21*, 343–346, 1986.

Buonsanto, M. J., A case study of the ionospheric storm dusk effect, *J. Geophys. Res., 100*, 23,857–23,869, 1995.

Burns, A. G., T. L. Killeen, and R. G. Roble, A theoretical study of thermospheric composition perturbations during an impulsive geomagnetic storm, *J. Geophys. Res., 96*, 14,153–14,167, 1991.

Burns, A. G., T. L. Killeen, G. R. Carignan, and R. G. Roble, Large enhancements in the O/N_2 ratio in the evening sector of the winter hemisphere during geomagnetic storms, *J. Geophys. Res., 100*, 14,661–14,671, 1995a.

Burns, A. G., T. L. Killeen, W. Deng, G. R. Carignan, and R. G. Roble, Geomagnetic storm effects in the low- to middle-latitude upper thermosphere, *J. Geophys. Res., 100*, 14,673–14,691, 1995b.

Burnside, R. G., C. A. Tepley, and V. B. Wickwar, The O^+-O collision cross-section: Can it be inferred from aeronomical measurements?, *Ann. Geophys., Ser. A, 5*, 343–350, 1987.

Chiu, Y. T., An improved phenomenological model of ionospheric density, *J. Atmos. Terr. Phys., 37*, 1563–1570, 1975.

Codrescu, M. V., R. G. Roble, and J. M. Forbes, Interactive ionosphere modeling: A comparison between TIGCM and ionosonde data, *J. Geophys. Res., 97*, 8591–8600, 1992.

Codrescu, M. V., T. J. Fuller-Rowell, and J. C. Foster, On the importance of *E*-field variability for Joule heating in the high-latitude thermosphere. *Geophys. Res. Lett., 22*, 2393–2396, 1995.

Craven, P. D., R. H. Comfort, P. G. Richards, and J. M. Grebowsky, Comparison of modeled N^+, O^+, H^+, and He^+ in the mid-latitude ionosphere with mean densities and temperatures from Atmospheric Explorer, *J. Geophys. Res., 100*, 257–268, 1995.

Crowley, G., B. A. Emery, R. G. Roble, H. C. Carlson Jr., and D. J. Knipp, Thermospheric dynamics during September 18–19, 1984, 1, Model simulations, *J. Geophys. Res., 94*, 16,925–16,944, 1989a.

Crowley, G., B. A. Emery, R. G. Roble, H. C. Carlson, Jr., J. E. Salah, V. B. Wickwar, K. L. Miller, W. L. OLiver, R. G. Burnside, and F. A. Marcos, Thermospheric dynamics during September 18–19, 1984, 2, Validation of the NCAR thermospheric general circulation model, *J. Geophys. Res., 94*, 16,945–16,959, 1989b.

Dalgarno, A., Ambipolar diffusion in the *F* region, *J. Atmos. Terr. Phys., 26*, 939, 1964.

Davis, C. J., A. D. Farmer, and A. Aruliah, An optimised method for calculating the O^+–O collision parameter from aeronomical measurements, *Ann. Geophys., 13*, 541–550, 1995.

Emery, B. A., et al., Assimilative mapping of ionospheric electrodynamics in the thermosphere-ionosphere general circulation model comparisons with global ionospheric and thermospheric observations during the GEM/Sundial period of March 28–29, 1992, *J. Geophys. Res.*, in press, 1996.

Evans, J. V., A study of F_2 region daytime vertical ionization fluxes at Millstone Hill during 1969, *Planet. Space Sci.*, *23*, 1461–1482, 1975.

Fesen, C. G., G. Crowley, and R. G. Roble, Ionospheric effects at low latitudes during the March 22, 1979, geomagnetic storm, *J. Geophys. Res.*, *94*, 5405–5417, 1989.

Fesen, C. G., R. G. Roble, and E. C. Ridley, Thermospheric tides at equinox: Simulations with coupled composition and auroral forcings, 2, Semidiurnal component, *J. Geophys. Res.*, *96*, 3663–3677, 1991.

Forbes, J. M., R. G. Roble, and F. A. Marcos, Thermospheric dynamics during the March 22, 1979, magnetic storm, 2, Comparisons of model predictions with observations, *J. Geophys. Res.*, *92*, 6069–6081, 1987.

Forbes, J. M., R. G. Roble, and C. G. Fesen, Acceleration, heating, and compositional mixing of the thermosphere due to upward propagating tides, *J. Geophys. Res.*, *98*, 311–321, 1993.

Foster, J. C., Storm time plasma transport at middle and high latitudes, *J. Geophys. Res.*, *98*, 1675–1689, 1993.

Foster, J. C., J. M. Holt, R. G. Musgrove, and D. S. Evans, Ionospheric convection associated with discrete levels of particle precipitation, *Geophys. Res. Lett.*, *13*, 656–659, 1986.

Fuller-Rowell, T. J., and D. S. Evans, Height integrated Pedersen and Hall conductivity patterns inferred from the TIROS-NOAA satellite data, *J. Geophys. Res.*, *92*, 7606–7618, 1987.

Fuller-Rowell, T. J., and D. Rees, A three-dimensional, time-dependent, global model of the thermosphere, *J. Atmos. Sci.*, *37*, 2545–2567, 1980.

Fuller-Rowell, T. J., and D. Rees, Derivation of a conservative equation for mean molecular weight for a two constituent gas within a three-dimensional, time-dependent model of the thermosphere, *Planet. Space Sci.*, *31*, 1209–1222, 1983.

Fuller-Rowell, T. J., D. Rees., S. Quegan, R. J. Moffett, and G. J. Bailey, Interactions between neutral thermospheric composition and the polar ionosphere using a coupled ionosphere-thermosphere model, *J. Geophys. Res.*, *92*, 7744–7748, 1987.

Fuller-Rowell, T. J., M. V. Codrescu, R. J. Moffett and S. Quegan, Response of the thermosphere and ionosphere to geomagnetic storms, *J. Geophys. Res.*, *99*, 3893–3914, 1994.

Garner, T. W., P. G. Richards, and R. H. Comfort, Anomalous nighttime electron temperature events over Millstone Hill, *J. Geophys. Res.*, *99*, 11,411–11,415, 1994.

Hagan, M. E., Quiet time upper thermospheric winds over Millstone Hill between 1984 and 1990, *J. Geophys. Res.*, *98*, 3731–3739, 1993.

Hedin, A. E., MSIS-86 thermospheric model, *J. Geophys. Res.*, *92*, 4649–4662, 1987.

Hedin, A. E, M. J. Buonsanto, M. Codrescu, M.-L. Duboin, C. G. Fesen, M. E. Hagan, K. L. Miller, and D. P. Sipler, Solar activity variations in midlatitude thermospheric meridional winds, *J. Geophys. Res.*, *99*, 17,601–17,608, 1994.

Heelis, R. A., J. K. Lowell, and R. W. Spiro, A model of the high-latitude ionospheric convection pattern, *J. Geophys. Res.*, *87*, 6339–6345, 1982.

Hernandez, G., and R. G. Roble, Thermospheric nighttime neutral temperature and winds over Fritz Peak Observatory: Observed and calculated solar cycle variation, *J. Geophys. Res.*, *100*, 14,647–14,659, 1995.

Khazanov, G. V., and M. W. Liemohn, Nonsteady state ionosphere-plasmasphere coupling of superthermal electrons, *J. Geophys. Res.*, *100*, 9669–9681, 1995.

Knipp, D. J., et al., Ionospheric convection response to slow, strong variations in a northward interplanetary magnetic field: A case study for January 14, 1988, *J. Geophys. Res.*, *98*, 19,273–19,292, 1993.

Lejeune, G., and F. Wormser, Diffusion of photoelectrons along a field line inside the plasmasphere, *J. Geophys. Res.*, *81*, 2900–2916, 1976.

Link, R., and L. L. Cogger, A reexamination of the O I 6300-Å nightglow, *J. Geophys. Res.*, *93*, 9883–9892, 1988.

Lu, G., A. D. Richmond, B. A. Emery, and R. G. Roble, Magnetosphere-ionosphere-thermosphere coupling: Effect of neutral winds on energy transfer and field-aligned current, *J. Geophys. Res.*, *100*, 19,643–19,659, 1995.

Maeda, S., T. J. Fuller-Rowell, and D. S. Evans, Zonally averaged dynamical and compositional response of the thermosphere to auroral activity during September 18–24, 1984, *J. Geophys. Res.*, *94*, 16,869–16,883, 1989.

Mantas, G. P., H. C. Carlson, and V. B. Wickwar, Photoelectron flux buildup in the plasmasphere, *J. Geophys. Res.*, *83*, 1–15, 1978.

Newberry, I. T., R. H. Comfort, P. G. Richards, and C. R. Chappell, Thermal He^+ in the plasmasphere: Comparison of observation with numerical calculations, *J. Geophys. Res.*, *94*, 15,265–15,276, 1989.

Oliver, W. L., Neutral and ion composition changes in the F region over Millstone Hill during the Equinox Transition Study, *J. Geophys. Res.*, *95*, 4129–4134, 1990.

Pesnell, W. D., K. Omidvar, and W. R. Hoegy, Momentum transfer collision frequency of O^+–O, *Geophys. Res. Lett.*, *20*, 1343–1346, 1993.

Quegan, S., G. J. Bailey, R. J. Moffett, R. A. Heelis, T. J. Fuller-Rowell, D. Rees, and R.W. Spiro, A theoretical study of the distribution of ionization in the high-latitude ionosphere and the plasmasphere: First results on the mid-latitude trough and the light-ion trough, *J. Atmos. Terr. Phys.*, *44*, 619–640, 1982.

Reddy, C. A., W. R. Hoegy, W. D. Pesnell, H. G. Mayr, and C. O. Hines, Accuracy of O^+–O collision cross-section deduced from ionosphere-thermosphere observations, *Geophys. Res. Lett.*, *21*, 2429–2432, 1994.

Richards, P. G., An improved algorithm for determining neutral winds from the height of the F_2 peak electron density, *J. Geophys. Res.*, *96*, 17,839–17,846, 1991.

Richards, P. G., D. G. Torr, M. J. Buonsanto, and D. P. Sipler, Ionospheric effects of the March 1990 magnetic storm: Comparison of theory and measurement, *J. Geophys. Res.*, *99*, 23,359–23,365, 1994a.

Richards, P. G., D. G. Torr, B. W. Reinisch, R. R. Gamache, and P. J. Wilkinson, F_2 peak electron density at Millstone Hill and Hobart: Comparison of theory and measurement at solar maximum, *J. Geophys. Res.*, *99*, 15,005–15016, 1994b.

Richards, P. G., J. A. Fennelly, and D. G. Torr, EUVAC: A solar EUV flux model for aeronomic calculations, *J. Geophys. Res.*, *99*, 8981–8992, 1994c. (Correction, *J. Geophys. Res.*, *99*, 13,283, 1994.)

Richmond, A. D. and Y. Kamide, Mapping electrodynamic features of the high-latitude ionosphere from localized observations: Technique, *J. Geophys. Res.*, *93*, 5741–5759, 1988.

Richmond, A. D., E. C. Ridley, and R. G. Roble, A thermosphere/ionosphere general circulation model with coupled electrodynamics, *Geophys. Res. Lett.*, *19*, 601–604, 1992.

Rishbeth, H., The effect of winds on the ionospheric F_2-peak, *J. Atmos. Terr. Phys.*, *29*, 225–238, 1967.

Robinson, R. M., R. R. Vondrak, K. Miller, T. Dabbs, and D. Hardy, On calculating ionospheric conductances from the flux and energy of precipitating electrons, *J. Geophys. Res.*, *92*, 2565–2569, 1987.

Roble, R. G., and E. C. Ridley, An auroral model for the NCAR thermospheric general circulation model (TGCM), *Ann. Geophys.*, *Ser. A*, *5*(6), 369–382, 1987.

Salah, J. E., Interim standard for the ion-neutral atomic oxygen collision frequency, *Geophys. Res. Lett.*, *20*, 1543–1546, 1993.

Salah, J. E., and J. V. Evans, Measurements of thermospheric temperatures by incoherent scatter radar, *Space Res. XIII*, 267–286, 1973.

Salah, J. E., and J. M. Holt, Midlatitude thermospheric winds from incoherent scatter radar and theory, *Radio Sci.*, *9*, 301–313, 1974.

Sipler, D. P., M. E. Hagan, M. E. Zipf, and M. A. Biondi, Combined optical and radar wind measurements in the F region over Millstone Hill, *J. Geophys. Res.*, *96*, 21,255–21,262, 1991.

Szuszczewicz, E. P., et al., F region climatology during the Sundial/ATLAS 1 campaign of March 1992: Model-measurement comparisons and cause-effect relationships, *J. Geophys. Res.*, in press, 1996.

Torr, M. R., D. G. Torr, P. G. Richards, and S. P. Yung, Mid- and low-latitude model of thermospheric emissions, 1, $O^+(^2P)$ 7320 Å, and $N_2(^2P)$ 3371 Å, *J. Geophys. Res.*, *95*, 21,147–21,168, 1990.

Young, E. R., P. G. Richards, and D. G. Torr, A flux preserving method of coupling first and second order equations to simulate the flow of plasma between the protonosphere and the ionosphere, *J. Comput. Phys.*, *38*, 141–156, 1980.

M. J. Buonsanto and D. P. Sipler, Massachusetts Institute of Technology, Haystack Observatory, Westford, MA 01886. (e-mail: mjb@oceanus.haystack.edu; dps@hyperion.haystack.edu)

M. Codrescu and T. J. Fuller-Rowell, Cooperative Institute for Research in Environmental Sciences, University of Colorado, Boulder, CO 80309. (e-mail: codrescu@sel.noaa.gov; tjfr@sel.noaa.gov)

B. A. Emery, High Altitude Observatory, NCAR, Boulder, CO 80307. (e-mail: emery@ncar.ucar.edu)

C. G. Fesen, W. B. Hanson Center for Space Sciences, University of Texas at Dallas, P. O. Box 830688, Richardson, TX 75083. (e-mail: cfesen@utdallas.edu)

D. J. Melendez-Alvira, Code 7643.1, Naval Research Laboratory, Washington, DC 20375. (e-mail: melendez@uap.nrl.navy.mil)

(Received April 1, 1996; revised August 2, 1996;
accepted August 20, 1996.)